Research Square

Preprints are preliminary reports that have not undergone peer review.
They should not be considered conclusive, used to inform clinical practice,
or referenced by the media as validated information.

A fractional-order Eulerian dispersion model with a single fractional order: formulation and evaluation against five tracer data sets

Antonio Goulart

antonio.goulart@furg.br

Universidade Federal do Rio Grande

Julian M. S. Suarez

Universidade Federal do Rio Grande

Joice C. Marques

Universidade Federal do Rio Grande

Adelaida O. Conza

Universidad Nacional del Altiplano

Matheus J. Lazo

Universidade Federal do Rio Grande

Research Article

Keywords:

Posted Date: November 19th, 2026

DOI: https://doi.org/10.21203/rs.3.rs-11394011/v1

License: This work is licensed under a Creative Commons Attribution 4.0 International License.
Read Full License

Additional Declarations: No competing interests reported.

A fractional-order Eulerian dispersion model with a single fractional order: formulation and evaluation against five tracer data sets

Antonio Goulart[1*], Julian M. S. Suarez[1], Joice C. Marques[1], Adelaida O. Conza[2], Matheus J. Lazo[1]

[1]Universidade Federal do Rio Grande, IMEF, Rio Grande, 96.201-900, RS, Brasil.
[2]Universidad Nacional del Altiplano, UNAP, Puno, 21001, Peru.

*Corresponding author(s). E-mail(s): antonio.goulart@furg.br;
Contributing authors: julian.sejje@furg.br; joicemtm@furg.br;
o.conzaadelaida@gmail.com; matheuslazo@furg.br;

Abstract

An Eulerian dispersion model for the planetary boundary layer is presented in which the vertical turbulent flux is written with a Caputo fractional derivative and, in three dimensions, the lateral flux with a symmetric Riesz operator. Dimensional consistency is provided by the vertical Lagrangian length scale of the turbulence, so that a single fractional order, common to all experiments, is the only quantity selected with reference to concentration data; all other parameterisations keep their published constants. The model, solved with a conservative finite-difference scheme, is evaluated against five tracer data sets (Copenhagen, convective and stable Prairie Grass, Hanford 83 and Kincaid) with statistical indices, bootstrap confidence intervals and the results of established models. In the classical limit the model performs at the level of those models. With a fractional order of 0.91 the fraction of predictions within a factor of two rises from 0.72 to 0.94 in convective Prairie Grass. A constant rescaling of the classical diffusivity reproduces this gain only in part and does not remove the growth of the residuals with distance. Copenhagen and Hanford 83 are statistically unchanged, while stable Prairie Grass and Kincaid deteriorate. The benefit is therefore restricted to surface releases in convective conditions.

Keywords: Atmospheric dispersion, Fractional advection–diffusion equation, Anomalous diffusion, Caputo derivative, Dispersion model evaluation, Prairie Grass

1 Introduction

Atmospheric dispersion models provide quantitative estimates of the spatial distribution of contaminants released into the planetary boundary layer (PBL), and their reliability depends primarily on the representation of turbulent transport. Operational modelling evolved from Gaussian plume solutions (Pasquill, 1974) to Eulerian formulations with vertically inhomogeneous wind and eddy-diffusivity profiles, solved by analytical, semi-analytical and numerical techniques (integral transforms, multi-layer discretisations, finite differences) (Degrazia, Campos Velho, & Carvalho, 1997; Kumar & Sharan, 2010, 2012; Moreira, Tirabassi, & Carvalho, 2005; Moreira, Vilhena, Buske, & Tirabassi, 2009), and to Lagrangian stochastic models (Carvalho, Vilhena, & Thompson, 2007). All the Eulerian formulations share the gradient-transfer (K-theory) closure, in which the turbulent flux is proportional to the local mean concentration gradient.

The vertical spreading of a passive scalar released near the surface of a convective boundary layer (CBL) is not described by this local closure over a substantial range of travel times. Water-tank experiments (Willis & Deardorff, 1976) and large-eddy simulations (Weil, Sullivan, Patton, & Moeng, 2012) show that the spreading is super-diffusive while the dimensionless travel time $X = x\, w_*/(\bar{u}\, h)$ is below $\sim$0.5, because organised thermals carry material across a large fraction of the mixed layer within a single eddy turnover. Two families of remedies coexist. The first keeps the integer-order equation and makes the closure non-local, through counter-gradient terms (Deardorff, 1966; Holtslag & Moeng, 1991) or transilient matrices (Stull, 1984). The second replaces integer-order derivatives by fractional ones (Goulart, Lazo, Suarez, & Moreira,

2017; Moreira, 2022; Moreira & Moret, 2018; Moreira, Xavier, Palmeira, & Nascimento, 2019), which amounts to a power-law kernel within the same class of integral closures, with the non-locality set by a single exponent.

The fractional route entered Eulerian dispersion modelling through Goulart et al. (2017), who placed a Caputo derivative of order α in the *advective* term and showed, on the Copenhagen campaign, that the fractional model with constant coefficients outperforms integer-order models with variable ones. Re-solving that equation by Laplace decomposition, Acioli, Xavier, and Moreira (2019) confirmed the gain for the elevated Copenhagen release but found that the same model *fails* for the convective surface releases of Prairie Grass, and closed by noting that "the fractional derivative is in the advective rather than the diffusive term ... a point to be investigated in the future". The diffusive placement was then adopted by Goulart, Lazo, and Suarez (2019), who wrote the turbulent concentration flux itself as a Caputo derivative and reported one order per stability regime across Copenhagen, Prairie Grass and Hanford 67; a local deformed (Hausdorff) derivative was later found to perform at the same level, with different orders, on the same data (Goulart, Lazo, & Suarez, 2020). In parallel, Moreira and co-workers developed the Jumarie-derivative branch (Moreira, 2022; Moreira & Moret, 2018; Moreira et al., 2019), and fractional Eulerian models have been applied to volcanic-ash transport (Troparevsky, Muszkats, Seminara, Zitto, & Piotrkowski, 2022) and to urban pollution (Madiyarov, Alimbekova, Bakishev, Mukhamediyev, & Yergaliyev, 2025). The fractional advection–dispersion equation has, moreover, two decades of history in subsurface hydrology, where it was introduced (Benson, Wheatcraft, & Meerschaert, 2000) and given the flux-form Eulerian derivation (Schumer, Benson, Meerschaert, & Wheatcraft, 2001) that the present model follows.

The fractional route has produced encouraging skill scores on convective tracer data, but three gaps limit what those scores establish and motivate the present study.

First, a fractional derivative of order $\alpha \neq 1$ changes the physical dimension of the term in which it appears. In the literature the imbalance has been absorbed into the fitted coefficient (Benson et al., 2000), closed by auxiliary lengths fixed at 1 m (Prates, Silva, Souza, & Moreira, 2022), bypassed by equating the advective and diffusive orders (Goulart et al., 2019), or avoided by adopting local deformed operators (Goulart et al., 2020; Silva, Xavier, & Moreira, 2025). The choice is rarely discussed, although the magnitude of the closing length determines the sign of the model's response to α (Section 2). Second, the order is frequently adjusted per experiment, per stability class or per model variant — published values for the same campaigns range from 0.54 to 0.99 according to the operator and its placement (Acioli et al., 2019; Goulart et al., 2019, 2020, 2017; Moreira, 2022) — which gives it one degree of freedom per subset; and performance claims, including our own, have generally been based on point values of statistical indices without significance analysis. Third, the numerical behaviour of the fractional operator on the stretched meshes that dispersion modelling requires is seldom reported, although the positivity and the stability of the discrete problem restrict the usable range of α as a function of the mesh.

In this work a steady-state Eulerian dispersion model, in two and three dimensions, is formulated with a Caputo derivative of order α in the vertical diffusive flux, closed dimensionally by the vertical Lagrangian length scale of Degrazia et al. (2000), and solved with a conservative finite-difference scheme. The parameterisations are taken from the literature with their published constants, and only the single order α — one value for all experiments — is selected with reference to concentration data. Following Chang and Hanna (2004) and Hanna and Chang (2012), the model is evaluated separately for each of five field data sets, with 95% confidence intervals computed for every performance measure by a block bootstrap that takes the experiment as the resampling unit (Efron, 1987; Hanna, 1989), with published acceptance criteria, and against the published indices of established Eulerian, semi-analytical and Lagrangian models.

2 Description of the dispersion model

2.1 The mathematical model

In a Cartesian coordinate system with the x axis aligned with the mean wind, the steady-state concentration field $c(x, y, z)$ of a passive scalar released from a continuous point source of strength Q at height H_s, in a horizontally homogeneous boundary layer of depth h with mean wind $u(z)$, obeys the advection–diffusion equation closed by the gradient-transfer hypothesis (Pasquill, 1974),

$$u(z)\frac{\partial c}{\partial x} = \frac{\partial}{\partial y}\Big(K_y \frac{\partial c}{\partial y}\Big) + \frac{\partial}{\partial z}\Big(K_z \frac{\partial c}{\partial z}\Big), \tag{1}$$

where K_y and K_z are the lateral and vertical eddy diffusivities and the longitudinal diffusive term is neglected relative to advection (the slender-plume approximation, valid when $K_x/(u\,x) \ll 1$, i.e. at large Péclet number, as holds at the source–receptor distances considered here). Since $\partial c/\partial y \to 0$ as $y \to \pm\infty$, integration over y eliminates the lateral term exactly and gives, for the crosswind-integrated concentration $\overline{c}^{\,y}(x, z) = \int_{-\infty}^{\infty} c\,\mathrm{d}y$, the two-dimensional equation

$$u(z)\frac{\partial \overline{c}^{\,y}}{\partial x} = \frac{\partial}{\partial z}\Big(K_z \frac{\partial \overline{c}^{\,y}}{\partial z}\Big), \tag{2}$$

which is the classical K-model against which the ground-level arc-integrated observations of the Prairie Grass, Copenhagen and Hanford campaigns are compared directly, with no assumption about the lateral spread.

As discussed in the Introduction, the gradient-transfer closure presupposes Fickian transport. To represent the non-local, anomalous vertical transport of the convective surface layer, the vertical turbulent flux is generalised here through a Caputo derivative of order α acting on the concentration, keeping the classical divergence outside the

memory integral:

$$u(z)\,\frac{\partial \overline{c}^{\,y}}{\partial x} = \ell^{\,\alpha-1}\,\frac{\partial}{\partial z}\left[K_z(z)\,\frac{\partial^{\alpha}\overline{c}^{\,y}}{\partial z^{\alpha}}\right], \qquad 0<\alpha\le 1, \tag{3}$$

where $\partial^{\alpha}/\partial z^{\alpha}$ is the Caputo derivative with lower terminal at the ground,

$$\frac{\partial^{\alpha} f}{\partial z^{\alpha}}(z) = \frac{1}{\Gamma(1-\alpha)}\int_0^{z}\frac{f'(\zeta)}{(z-\zeta)^{\alpha}}\,\mathrm{d}\zeta, \tag{4}$$

and ℓ is a reference length discussed below. For $\alpha = 1$, Eq. (3) reduces exactly to the classical Eq. (2). Equation (3) is subject to zero diffusive flux at the ground and at $z = h$, and to the source condition

$$K_z\frac{\partial^{\alpha}\overline{c}^{\,y}}{\partial z^{\alpha}} = 0 \;\text{ at }\; z = z_0,\; z = h, \qquad u\,\overline{c}^{\,y}(0,z) = Q\,\delta(z-H_s), \tag{5}$$

where z_0 is the roughness length and $\delta(\cdot)$ the Dirac delta.

The three-dimensional model, needed for the campaigns that publish arc-maximum concentrations rather than arc integrals, adds a lateral term with the *symmetric* Riesz–Caputo operator,

$$u(z)\,\frac{\partial c}{\partial x} = \ell^{\,\alpha-1}\left\{\frac{\partial}{\partial y}\left[K_y\,D^{\alpha}_{y,R}\,c\right] + \frac{\partial}{\partial z}\left[K_z\,\frac{\partial^{\alpha}c}{\partial z^{\alpha}}\right]\right\}, \qquad D^{\alpha}_{y,R} = \tfrac{1}{2}\left(D^{\alpha}_{y,+} + D^{\alpha}_{y,-}\right), \tag{6}$$

with zero-flux conditions on all lateral and vertical boundaries. The lateral operator must be symmetric because the plume axis is a symmetry axis and the lateral boundaries are artificial: a one-sided derivative anchors the memory to an arbitrary domain edge and makes the solution depend on where the domain is cut, whereas the Riesz form is symmetric to 10^{-12} and insensitive to the lateral domain size. The three-dimensional fractional solution of Tankou Tagne, Ele Abiama, Ema'a Ema'a,

Owono Ateba, and Ben-Bolie (2021) places the fractional derivative in the advective term and keeps classical operators in both transverse directions; to our knowledge, Eq. (6) is the first three-dimensional dispersion model with the non-local operator in the diffusive fluxes.

Dimensional consistency and the reference length

For $\alpha \neq 1$ the fractional derivative of the concentration has dimension $[c]\,\mathrm{L}^{-\alpha}$, so the diffusion term in Eq. (3) balances only if it is multiplied by a length to the power $\alpha - 1$. The magnitude of this length matters: for the present configuration, values of ℓ below a threshold $\ell^* \approx 16$–19 m make the plume *wider* as α decreases, and values above it make the plume *narrower*. A model that closes the dimension with a unit constant therefore fixes the sign of its response to α implicitly. Here ℓ is the layer-averaged vertical Lagrangian length scale ℓ_w of Degrazia et al. (2000) (Section 3.5), evaluated per experiment from the tabulated micrometeorology and never adjusted; across the five data sets it spans 0.04–567 m.

Structural properties of the operator choice

Three properties, independent of any data set, determine the remaining choices in Eqs. (3)–(6). (i) *Positivity.* A fractional derivative multiplied by a spatially varying diffusivity can violate positivity: for constant K the semi-discrete operator is a Markov generator for every α tested, whereas for variable K positivity fails on the side whose memory originates in the region of smaller K, with a violation that grows linearly in $(1 - \alpha)$. Since K_z increases away from the ground, the left-sided vertical operator of Eq. (4) is affected; the lateral term is not, because K_y does not depend on y. (ii) *Caputo rather than Riemann–Liouville flux.* On a bounded interval with reflecting conditions the Riemann–Liouville flux relaxes to a steady state that is singular at the boundary where the memory is anchored, whereas the Caputo-flux form relaxes to the well-mixed profile (Baeumer, Kovács, Meerschaert, & Sankaranarayanan, 2018; Kelly,

Sankaranarayanan, & Meerschaert, 2019), which is the physical limit for a scalar over an impermeable ground; our discrete solutions reproduce both behaviours. (iii) *Lateral width.* The lateral operator in Eq. (6) has total order $1+\alpha \in (1,2)$, so the second moment of the lateral profile diverges for $\alpha < 1$; the lateral width of the model is therefore computed as that of the data is, $\sigma_y = \bar{c}^{\,y}/(\sqrt{2\pi}\, c_{\max})$.

2.2 The numerical model

Equation (3) is marched implicitly in x on a non-uniform vertical mesh z_k generated by an arctangent stretching, fine near the ground in order to resolve the surface releases (0.46 m at Prairie Grass). Three ingredients make conservation exact. *Flux form.* The diffusion term is discretised as a difference of fractional fluxes at the cell faces, $F_{k+1/2} = -K_{k+1/2}\,(\partial^\alpha c/\partial z^\alpha)|_{z_{k+1/2}}$, with $F_{-1/2} = F_{N+1/2} = 0$; the telescoping sum then makes $\sum_k u_k \bar{h}_k c_{ik} = Q$ an algebraic identity of the scheme at every station i and for every α, which extends to variable K_z and non-uniform meshes the conservation property known for constant coefficients (Kelly et al., 2019). *Consistent L1 quadrature.* The Caputo derivative at the faces uses an L1-type quadrature written for the actual non-uniform mesh, including the final partial interval,

$$\frac{\partial^\alpha c}{\partial z^\alpha}(\zeta) \simeq \frac{1}{\Gamma(2-\alpha)} \sum_j s_j \left[(\zeta - z_j)^{1-\alpha} - \big(\zeta - \min(z_{j+1}, \zeta)\big)^{1-\alpha} \right], \tag{7}$$

with $s_j = (c_{j+1} - c_j)/(z_{j+1} - z_j)$. Equation (7) is the L1 approximation of Lin and Xu (2007), whose $O(\Delta^{2-\alpha})$ truncation and positive, monotonically decreasing weights are established on uniform meshes; on non-uniform meshes both properties hold only if the weights are the exact kernel averages on the actual mesh (Kopteva, 2019), as in Eq. (7). At $\alpha = 1$ Eq. (7) reduces analytically to the classical flux-form scheme, so the classical limit is recovered exactly. *Conservative source.* The point source is distributed over the two cells bracketing H_s, with weights chosen so that the discrete

flux equals Q at $x = 0$. The reference mesh has 640 stations in x and 160 levels in z; the three-dimensional solver uses the same vertical operator, the Riesz lateral operator on a tangent-mapped lateral mesh of 192 nodes, and a marching scheme diagonalised in the lateral eigenbasis; where K_y depends on x (stable branch) the domain is split into 32 blocks with K_y frozen per block (block-convergence error 0.05%).

The verification suite (Table 1) gives the following. Conservation holds to $|\Phi/Q - 1| \leq 5 \times 10^{-14}$ (2-D) and $\leq 8 \times 10^{-10}$ (3-D, all cases); the integral over y of the 3-D field reproduces the 2-D solution to 10^{-12} — the lateral term telescopes to zero, so the 3-D solver is pinned to the independently verified 2-D solver; mesh refinement at fixed stretching changes the reported concentrations by less than 0.31% in the worst campaign; and the classical limit is exact.

Table 1 Verification suite. Φ is the discrete flux $\sum u\bar{h}c$; "mesh doubling" reports the worst relative change of any compared concentration when each mesh parameter is doubled separately at fixed stretching.

Test	Criterion	Result
Mass conservation, 2-D	$\lvert\Phi/Q - 1\rvert$, all x, all α	$\leq 5 \times 10^{-14}$
Mass conservation, 3-D	idem	$\leq 8 \times 10^{-10}$
3-D pinned to 2-D	$\lvert \int c\,\mathrm{d}y - \bar{c}^{\,y}_{2D}\rvert / \bar{c}^{\,y}$	$\leq 2 \times 10^{-12}$
Classical limit	$\alpha = 1$ vs. integer-order solver	exact
Lateral symmetry (Riesz)	max asymmetry	10^{-12}
Mesh doubling (L, M, N, β_y, L_y, blocks)	worst case	0.31%
Quadrature order (stretched mesh)	observed order	1.4–1.6

The usable range of α depends on the mesh

Because positivity is lost through the product of the memory kernel with a K_z that varies over the memory span, the smallest off-diagonal element of the implicit-step matrix becomes more negative as the vertical mesh is refined. On the reference mesh (640×160) the discrete operator preserves positivity down to $\alpha \approx 0.93$; on a mesh twice as fine the marching *diverges* for $\alpha \leq 0.87$ in the deepest CBL experiments, and the

violation grows by a fixed factor per doubling (≈ 34, identical across experiments), so that refinement does not restore positivity. The mechanism is specific to the *conservative* placement of the variable coefficient: when the coefficient multiplies the fractional operator from outside, the implicit shifted-Grünwald scheme is unconditionally stable (Meerschaert & Tadjeran, 2004), whereas for the flux form $\partial_z[K_z(z)\,\partial_z^\alpha c]$, required for exact conservation, the stability theory remains open even in one dimension (Kong & Fu, 2024). The usable range of α is therefore a property of the operator–mesh pair and must be reported together with the mesh. All results in this paper were obtained on the reference mesh, on which the march is stable and conservative at the operating value $\alpha = 0.91$ (Section 4.3); this value lies slightly below the positivity bound of that mesh, which must be kept in mind when the results for $\alpha < 1$ are interpreted.

3 Turbulence parameterizations

The inputs of the present model are published parameterisations with their published constants; none was adjusted to the dispersion data, and the single structural change made (the stable lateral length scale, Section 3.3) is stated explicitly. The stable and convective regimes use different diffusivities, both derived from Taylor's statistical diffusion theory combined with spectral models of the turbulence (Degrazia et al., 2000, 1997; Degrazia & Moraes, 1992).

3.1 Stable and near-neutral boundary layer

For the stable and near-neutral regimes the local-similarity eddy diffusivity of Mangia et al. (2002, Eq. 16) is adopted,

$$K_z = \frac{0.3\,(1 - z/h)\,u_* z}{1 + 3.7\,z/\Lambda}, \qquad \Lambda = L\,(1 - z/h)^{5/4}, \tag{8}$$

where u_* is the surface friction velocity, L the Obukhov length, h the stable boundary layer height and Λ the local Obukhov length of the local-scaling hypothesis (Degrazia & Moraes, 1992; Sorbjan, 1986). The results are insensitive to the published variants of this functional form (surface or local scaling of u_*, and the h-independent form $0.3\,u_* z/(1+3.7z/L)$): over the stable Prairie Grass set the FA2 changes by at most one pair among them. The stable boundary layer heights of the data sets used here are not measured: the tabulated values are reproduced to within 5% by the diagnostic relation $h = 0.4\,(u_* L/f)^{1/2}$ of Zilitinkevich (1972), where f is the Coriolis parameter.

Equation (8) was adopted before the fractional order was examined and kept fixed throughout.

3.2 Convective boundary layer

In convective conditions the vertical eddy diffusivity derived from spectral properties by Degrazia et al. (1997) is used,

$$\frac{K_z}{w_* h} = 0.22\left(\frac{z}{h}\right)^{1/3}\left(1-\frac{z}{h}\right)^{1/3}\left[1-\exp\!\left(-\frac{4z}{h}\right)-0.0003\exp\!\left(\frac{8z}{h}\right)\right], \qquad (9)$$

where w_* is the convective velocity scale and h ($\equiv z_i$) the convective boundary layer height. Where the campaign tabulates w_*, L and h but not u_* (convective Prairie Grass), the friction velocity that drives the wind profile is the one implied by the definitions of L and w_*, $u_* = w_*(-\kappa L/h)^{1/3}$, so that advection and turbulent closure are driven by mutually consistent measured scales.

3.3 Lateral eddy diffusivity (three-dimensional model)

Two published forms are used, selected by regime and both based on Taylor's statistical theory. In convective conditions the lateral diffusivity of Moreira et al. (2005, Eq. 18) is adopted, with its published constants ($c_v = 0.36$, $\psi = 0.4$) and the lateral peak

wavelength $(\lambda_m)_v = 1.5\,h$ of Degrazia et al. (2000, Eq. 17); it tends to $K \propto x$ near the source (Sharan, Yadav, & Modani, 2002) and to the asymptotic K_∞ of Degrazia et al. (2000, Eq. 15) far from it. In stable conditions the analogous published forms carry a lateral length scale proportional to z, which vanishes at the ground and gives $\ell_v \sim 0.3$ m at the Prairie Grass sampling height, whereas the observed lateral widths require $\ell_v = \sigma_v T_L \approx 20$–$30$ m. Because the ground blocks vertical but not lateral motions, the lateral energy-containing wavelength should not vanish at the surface — as Degrazia et al. (2000) assume for the CBL (their Eq. 17) — and the same structure is used here for the stable branch, $\ell_v^{(s)} = 0.2016\,h/(1 + 3.7z/\Lambda)$, with $K = \sigma_v \ell_v$, $T_L = \ell_v/\sigma_v$ and the interpolation of Kumar and Sharan (2010); Mooney and Wilson (1993). This is the only modification of a published parameterisation in this work. It introduces no constant fitted to concentrations, but it was motivated by the observed lateral widths of the stable Prairie Grass runs, for which the FA2 of the width $\sigma_y = \bar{c}^{\,y}/(\sqrt{2\pi}\,c_{\max})$ changes from 0.013 to 0.720. It affects only the arc-maximum concentrations of the stable three-dimensional runs: the crosswind-integrated results, on which α was selected, do not depend on K_y.

3.4 The mean wind profile

The mean wind is described by the same Monin–Obukhov surface-layer similarity profile in both regimes, with the flux–profile constants of Businger, Wyngaard, Izumi, and Bradley (1971) in the integrated form of Paulson (1970),

$$u(z) = \frac{u_*}{\kappa}\left[\ln\frac{z}{z_0} - \psi_m\!\left(\frac{z}{L}\right)\right], \tag{10}$$

$$\psi_m = \begin{cases} -4.7\,z/L, & L > 0, \\ \ln\dfrac{1+X^2}{2} + 2\ln\dfrac{1+X}{2} - 2\arctan X + \dfrac{\pi}{2}, & L < 0, \end{cases} \tag{11}$$

with $X = (1 - 15z/L)^{1/4}$ and $\kappa = 0.4$; the profile is held constant above $z_b = \min(|L|, 0.1h)$, the customary cutoff of the Eulerian models from which this work descends (Moreira & Moret, 2018; Panofsky & Dutton, 1984). The profile contains no adjustable parameter and is driven by the same friction velocity that enters K_z. Where a campaign reports both u_* and a wind speed at a reference height, the two are not always mutually consistent; here u_* is retained and the profile is *not* rescaled to the observed wind. Because the transport wind affects every concentration, this convention was checked against primary data. The Prairie Grass central mast recorded 20-min wind profiles at seven heights (0.25–16 m) during every run (Barad, 1958, Vol. I, Table 8.1); Eq. (10) reproduces the measured wind at all levels from 0.5 to 16 m, with median ratio 0.97 (10th–90th percentiles 0.94–0.99; 113 model–mast pairs) for the 20 convective runs and 0.92 (0.85–1.03; 138 pairs) for the 23 clean stable runs, the latter uniformly in height, which indicates an offset in u_* rather than an error in the shape of the profile. The same data show that the "U_{10}" tabulated for the stable Prairie Grass runs in the compilations used here and in earlier Eulerian studies is 0.79 (0.74–0.81 on the clean set) of the 10-m mast wind and coincides with the mast wind at 4 m, whereas the convective tabulated values agree with the 10-m mast wind (0.98). For Hanford 83 the profile is driven by the u_* and L published per run in the primary source (Doran & Horst, 1985, Table 1), which gives no 2-m anemometer wind. The consequences of alternative wind conventions are summarised in Section 5.3.

3.5 The reference length

The reference length ℓ of Eqs. (3)–(6) is the vertical Lagrangian length scale ℓ_w of Degrazia et al. (2000), Eq. (24) in the convective branch and Eq. (25) in the neutral/stable branch, averaged over the layer,

$$\ell = \frac{1}{h}\int_0^h \ell_w(z)\,\mathrm{d}z, \tag{12}$$

and evaluated per experiment from the tabulated u_*, w_*, L and h. It is the length scale of the energy-containing eddies in the same spectral model that yields K_z, which makes it a natural scale for the non-local vertical transport represented by Eq. (3).

Adjustable quantities

The constants of the parameterisations above are those of the cited papers, ℓ is computed from the tabulated micrometeorology, and the wind profile follows similarity theory without rescaling. The fractional order is the only quantity selected with reference to concentration data: a single value, common to all experiments, chosen from the four classical data sets (Section 4.3) and then held fixed for the evaluation on Kincaid.

4 Field data and evaluation methodology

The model is evaluated against five tracer data sets: Copenhagen (Gryning & Lyck, 1984) and the convective Prairie Grass runs (Barad, 1958) (elevated and surface releases in the convective boundary layer), Kincaid (Bowne & Londergan, 1983) (a buoyant tall-stack release in convective conditions), and the stable Prairie Grass runs and Hanford 83 (Doran & Horst, 1985) (surface releases in the stable boundary layer). The compared quantity is the crosswind-integrated ground-level concentration $\bar{c}^{\,y}$ (two-dimensional model) where the campaign provides it, and the arc-maximum concentration $c_{\max}$ at the sampling height (three-dimensional model) otherwise. The tracers are treated as conserved (no deposition or chemical loss).

4.1 Field experiments

4.1.1 Copenhagen experiment

The Copenhagen campaign was carried out in 1978 in the northern suburban area of Copenhagen and is documented by Gryning and Lyck (1984). A non-buoyant tracer (SF_6) was released continuously from a tower at a height of 115 m and sampled

at ground level along crosswind arcs at 2–6 km from the source, with 1-h sampling intervals; the site was mainly residential, with a roughness length of about 0.6 m, and the conditions ranged from near-neutral to moderately convective. Nine runs provide 23 observation–prediction pairs, for which both the crosswind-integrated concentration and the arc maximum are tabulated. The meteorological data of the Copenhagen experiments are listed in Table S1 (Online Resource 1).

4.1.2 Prairie Grass experiment

The Prairie Grass experiment (Barad, 1958) was carried out in O'Neill, Nebraska, in 1956, and remains the most widely used surface-release dispersion data set. The tracer (SO_2) was released without buoyancy at a height of 0.46 m and sampled at 1.5 m along crosswind arcs at 50, 100, 200, 400 and 800 m; the site was flat and smooth, with a roughness length of 0.6 cm. For the convective runs the 20-run selection with the micrometeorology and crosswind-integrated concentrations compiled by Gonçalves, Quadros, and Buske (2013) is used — the same selection used by the models compared against — at the five arcs (100 pairs); arc maxima are tabulated for 19 of the 20 runs (95 pairs). The stable set comprises 25 runs at the 50, 200 and 800 m arcs (75 pairs, with both $\bar{c}^{\,y}$ and $c_{\max}$). Runs 13 and 14 are anomalous (non-monotonic arc maxima in one; $u_*/U_{10} = 0.014$ in the other, values known to be problematic in this data set), and all stable results are reported both for the full set and for the 23-run clean set. The boundary layer height h of the stable runs is the diagnosed height of the ground-based stable layer (Section 3.1), whereas in convective conditions it is the mixed-layer depth; for the convective runs the friction velocity, which drives the wind profile, was obtained from w_*, h and L (Section 3.2). The meteorological data from the convective and stable Prairie Grass experiments are listed in Table S2 and Table S3, respectively (Online Resource 1).

4.1.3 Hanford 83 experiment

The Hanford diffusion experiment (Doran & Horst, 1985) took place in May–June 1983 on the Hanford site, a flat, semi-arid steppe region of southeastern Washington with a roughness length of about 3 cm and a sagebrush canopy (displacement height 1.4 m). Six dual-tracer releases were performed under moderately stable to near-neutral conditions; the non-depositing SF_6 tracer was released at 2 m at about 0.3 g s^{-1} and sampled at 1.5 m on arcs at 100, 200, 800, 1600 and 3200 m (30 pairs of crosswind-integrated concentration normalised by the emission rate). The meteorological data of the Hanford 83 experiments are listed in Table S4 (Online Resource 1).

4.1.4 Kincaid experiment

The Kincaid experiment (Bowne & Londergan, 1983) involved a buoyant release of SF_6 from the 187-m stack of the Kincaid power plant (Illinois) in 1980–81, sampled on arcs from 1 to 50 km in convective conditions; its quality-screened data set is a standard benchmark for operational models. The 53 hourly experiments used here, with their micrometeorology (u_*, w_*, L, h), stack parameters and emission, coincide with the hourly records of the Model Validation Kit (Olesen, 2005), against which they were checked (one experiment carries the predicted rather than the observed mixing height, and four lack tower winds; neither affects the statistics below); 166 quality-screened pairs of arc-maximum concentration normalised by the emission rate are compared. Plume rise is computed with the Briggs (1975) formulae (final rise as the minimum of the momentum, touchdown, breakup and geometric limits), and the effective source height $h_e = H_s + \Delta h$ has median $h_e/h = 0.62$. The micrometeorological parameters of the 53 experiments are listed in Table S5 (Online Resource 1).

4.2 Statistical evaluation methodology

To quantify the agreement between modelled and observed concentrations, the statistical indices recommended by Hanna (1989) and Chang and Hanna (2004) were employed:

$$
\begin{aligned}
\textit{NMSE}\ \text{(normalized mean-square error)} &= \frac{\overline{(C_o - C_p)^2}}{\overline{C_o}\;\overline{C_p}}, \\
\textit{Cor}\ \text{(correlation coefficient)} &= \frac{\overline{(C_o - \overline{C_o})(C_p - \overline{C_p})}}{\sigma_o \sigma_p}, \\
\textit{FB}\ \text{(fractional bias)} &= \frac{(\overline{C_o} - \overline{C_p})}{0.5(\overline{C_o} + \overline{C_p})}, \\
\textit{FS}\ \text{(fractional standard deviation)} &= \frac{\sigma_o - \sigma_p}{0.5(\sigma_o + \sigma_p)},
\end{aligned}
$$

where C_p denotes the predicted and C_o the observed concentration, σ_p and σ_o their standard deviations, and the overbar an arithmetic mean. The additional measure *FA*2 is the fraction of pairs satisfying $0.5 \leq C_p/C_o \leq 2$. Optimal performance is indicated by *NMSE*, *FS* and *FB* approaching zero and by *Cor* and *FA*2 approaching unity; a positive FB denotes underprediction.

Following Hanna (1989), 95% confidence intervals were estimated for every index of the proposed model by bootstrap resampling (Efron, 1987), with one refinement imposed by the structure of the data: the arcs of a single run share its micrometeorology and are not independent, and the run-to-run variability of dispersion is itself large (Weil et al., 2012), so the resampling unit is the *experiment* (block bootstrap), not the individual observation–prediction pair. The experiments of each campaign were resampled with replacement 10 000 times, the indices recomputed for each resample, and the confidence limits taken from the 2.5th and 97.5th percentiles. Differences between two configurations of the model (the fractional order against its classical limit, or one wind-profile convention against another) are always *paired*: the same resample enters both terms, so the common sampling variability cancels and the interval applies

to the difference itself, as recommended by Chang and Hanna (2004). In addition, the acceptance criteria consolidated by Hanna and Chang (2012) for rural field data were applied: a model is considered acceptable when $|FB| \leq 0.30$, $NMSE \leq 3$ and $FA2 \geq 0.5$, with at least half of the individual criteria satisfied in each experiment.

Two caveats must be stated explicitly. First, since only the published point values of the indices are available for the literature models, the comparisons below are based on whether those published values fall inside the 95% confidence intervals of the corresponding measures of the proposed model; this is an approximate criterion, used here only to avoid unsupported claims of superiority, and where a published study retained a different subset of runs the comparison is one of level, not a paired test. Second, the fractional order was fixed on the four classical data sets (Section 4.3); the indices reported for those campaigns at $\alpha < 1$ are therefore in-sample measures, whereas the Kincaid results were obtained with α held fixed and are out-of-sample.

Use of artificial intelligence. A large language model (Claude, Anthropic) was used, under the direction of the authors, to assist in writing and testing the numerical code, in running the statistical analyses and in drafting and revising the text of this article. The equations, the numerical results and the statements made here were checked by the authors, who take full responsibility for the content.

4.3 Comparison models and the fractional order

The proposed model is compared with indices published for the same data sets by established models: the Lagrangian model of Carvalho et al. (2007), based on a semi-analytical solution of the Langevin equation; the Eulerian solutions of Kumar and Sharan (2012), with a height-dependent eddy diffusivity, and of Kumar and Sharan (2010), with a diffusivity depending on distance and height (Hanford); the Laplace-transform solution of Moreira, Carvalho, and Goulart (2002); and the GILTT and ADMM solutions of Moreira et al. (2009). For Kincaid the published evaluations are

the GILTT solution (Buske, 2008), the Gaussian model with plume rise of Moreira et al. (2004) and the three-dimensional non-local GIADMT solution (Costa, Vilhena, Moreira, & Tirabassi, 2006) with two values of the skewness parameter. For the strongly convective Prairie Grass runs the fractional model of Moreira (2022) — Jumarie-type derivatives in the advective and diffusive terms; its 19-run subset ($-h/L > 10$) coincides with ours, so that comparison is a paired one.

For the proposed model the fractional order is a single value common to all experiments. It was selected from the four classical data sets (Copenhagen, the two Prairie Grass sets and Hanford 83) by examining the response of the pooled crosswind-integrated statistics to α on the reference mesh: over the 228 pairs, FA2 rises from 0.737 at $\alpha = 1$ to 0.807 at $\alpha = 0.91$, a paired block-bootstrap gain of $+0.070$ $[+0.017; +0.122]$, while the pooled correlation is essentially unchanged; $\alpha = 0.93$ gives $+0.053$ $[+0.022; +0.083]$. The value $\alpha = 0.91$ was adopted and held fixed for Kincaid. As Section 5.1 shows, the pooled gain originates in the convective Prairie Grass runs. Alternative placements of the operator were examined in the same way and perform worse: a fractional advective term gives no significant pooled gain; the two-sided (Riesz) vertical operator gives $+0.018$ $[-0.009; +0.043]$; and a right-sided vertical Caputo derivative degrades the aggregate (-0.040 $[-0.066; -0.013]$). The gain is thus specific to left-sided vertical memory in the diffusion term, that is, to memory anchored at the ground.

5 Results and discussion

5.1 Model performance

5.1.1 Convective regime: Copenhagen

Table 2 presents the statistical indices for the Copenhagen experiment at $\alpha = 1$ and $\alpha = 0.91$, with the block-bootstrap 95% confidence intervals and the published indices

of the comparison models (scatter diagram in Fig. 1). The acceptance criteria are satisfied at both orders ($|FB| = 0.05$ and 0.11, $NMSE = 0.06$ and 0.07, $FA2 = 1.00$): all 23 predictions fall within a factor of two of the observations, and the correlation (0.91, CI [0.81, 0.97]) is at the level of the reference models. The fractional order has no effect that the data can resolve: FA2 does not change, the correlation changes by $+0.002$ $[-0.020; +0.046]$, and the only significant paired difference is a small increase of the fractional bias ($+0.054$ $[+0.040; +0.066]$), i.e. a slightly stronger underprediction of the arc integrals. Apart from the fractional bias of the GILTT solution (-0.14) and the FA2 of Kumar and Sharan (0.96, against an interval that is degenerate because FA2 saturates), the published indices of the comparison models lie within the 95% confidence intervals of the proposed model, so the five formulations are statistically indistinguishable on this data set.

Table 2 Statistical indices for the Copenhagen experiment (crosswind-integrated ground-level concentration, 23 pairs; this work: Eqs. 3 and 9). Values in brackets are block-bootstrap 95% confidence intervals for the proposed model (experiment as resampling unit, 10 000 replicas). *Lagrangian model.

Model	Cor	NMSE	FS	FB	FA2
This work, $\alpha = 1$ (classical limit)	0.908	0.058	+0.203	+0.052	1.000
95% CI	[0.81, 0.97]	[0.03, 0.10]	[−0.02, +0.38]	[−0.07, +0.17]	[1.00, 1.00]
This work, $\alpha = 0.91$	0.910	0.069	+0.207	+0.106	1.000
95% CI	[0.85, 0.97]	[0.03, 0.11]	[−0.06, +0.39]	[−0.02, +0.22]	[1.00, 1.00]
Carvalho et al. (2007)*	0.94	0.03	+0.02	+0.05	1.00
Kumar and Sharan (2012)	0.90	0.05	+0.34	-0.04	0.96
Moreira et al. (2009), GILTT	0.92	0.06	-0.02	-0.14	1.00
Moreira et al. (2009), ADMM	0.89	0.06	+0.09	+0.02	1.00

5.1.2 Convective regime: Prairie Grass

Table 3 presents the indices for the 20 convective Prairie Grass runs (100 pairs) and Fig. 2 the corresponding scatter diagram. At $\alpha = 1$ the model satisfies the three acceptance criteria ($|FB| = 0.15$, $NMSE = 0.08$, $FA2 = 0.72$), with a correlation (0.978, CI [0.971, 0.985]) and an NMSE (0.076, CI [0.05, 0.10]) at the level of the best

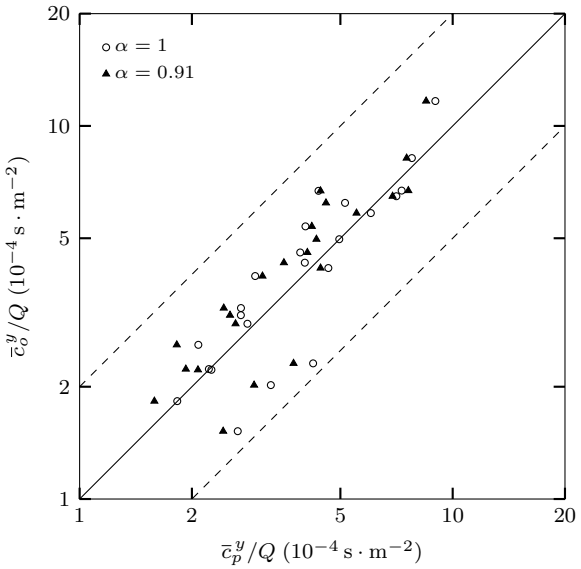


Fig. 1 Predicted ($\bar{c}_p^y/Q$) versus observed ($\bar{c}_o^y/Q$) normalised crosswind-integrated ground-level concentrations for the Copenhagen experiment, computed with the proposed model at $\alpha = 1$ (open circles) and $\alpha = 0.91$ (filled triangles). The solid line represents perfect agreement and the dashed lines the factor-of-two bounds.

values in the table. However, like the classical comparison models (FA2 = 0.68–0.81), it places only 72% of the pairs within a factor of two, and it overpredicts the arc integrals ($FB = -0.15$, CI $[-0.18, -0.12]$). At $\alpha = 0.91$ FA2 rises to 0.94 (CI [0.87, 0.99]), a paired gain of +0.220 $[+0.140; +0.300]$, and the bias changes sign and decreases in magnitude ($FB = +0.08$, CI $[+0.04, +0.12]$; paired change +0.224 $[+0.204; +0.247]$). The correlation is unchanged (0.975; paired change -0.003 $[-0.011; +0.005]$); NMSE rises from 0.076 to 0.104, a change whose paired interval ($+0.028$ $[-0.004; +0.072]$) includes zero, and FS increases from +0.14 to +0.22. These last two changes reflect the fact that the left-sided memory operator lowers the near-source concentrations most, so that the largest observations, which dominate NMSE and FS, are reproduced slightly less closely while most pairs move into the factor-of-two band (Fig. 2).

At $\alpha = 0.91$ the FA2 of the proposed model (0.94) exceeds the published values of the four classical comparison models (0.68–0.81), which fall below its lower confidence limit, and the fractional bias (+0.08) is within the range reported for the Eulerian

models (+0.03 to +0.16). The NMSE of the Lagrangian model of Carvalho et al. (2007) lies inside the confidence interval of the proposed model and its correlation (0.96) is marginally below the lower limit (0.97), so no difference of practical significance can be claimed for those measures. The comparison with the fractional model of Moreira (2022) is made on the same 19 strongly convective runs ($-h/L > 10$, 95 pairs; last two rows of Table 3, whose indices refer to that subset). On that subset the classical limit of the present model gives $NMSE = 0.076$, $Cor = 0.977$, $FA2 = 0.726$ and $FB = -0.154$, close to Moreira's classical benchmark, and $\alpha = 0.91$ gives 0.084, 0.978, 0.947 and +0.061, against his 0.07, 0.99, 0.96 and +0.13 obtained with two fractional orders. Two codes with different operators, numerical methods and K_z thus reproduce the same classical level and a similar fractional gain in FA2 at essentially unchanged correlation.

The gain occurs where non-local transport is expected (Section 1): 93 of the 95 convective pairs with arc maxima have $X < 0.5$, within the super-diffusive range of the tank experiments of Willis and Deardorff (1976), and a left-sided memory anchored at the ground is consistent with material carried upward by organised thermals from a surface source. This interpretation is nevertheless indirect: it rests on concentration statistics, and the order was selected on data that include these runs (Section 4.2). Section 5.2 shows that the gain persists in the arc-maximum concentrations of the three-dimensional model.

Classical control. To test whether this gain amounts to a rescaling of the eddy diffusivity, the classical model ($\alpha = 1$) was rerun for the convective Prairie Grass runs with K_z multiplied by a constant factor f between 0.5 and 3, everything else unchanged (Table 4). A larger diffusivity does raise FA2: it is 0.84 at $f = 1.35$, the factor that reproduces the fractional bias obtained with $\alpha = 0.91$ ($FB = +0.08$), and it reaches a plateau of 0.90–0.92 for $f = 1.45$–2.0, but there with $FB = +0.14$ to +0.42 and $NMSE = 0.16$ to 0.54, against +0.08 and 0.10 at $\alpha = 0.91$. The paired difference

in FA2 between $\alpha = 0.91$ and the rescaled classical model is $+0.10$ $[+0.03; +0.17]$ at equal bias and $+0.04$ $[0.00; +0.09]$ at $f = 1.5$; at $f = 1.9$ it is no longer significant ($+0.02$ $[-0.03; +0.07]$), while NMSE and bias are significantly worse ($NMSE$ 0.45 against 0.10). Most of the FA2 gain can thus be obtained by rescaling K_z, but only by replacing the classical overprediction with an underprediction of similar or larger magnitude. The two modifications differ in their dependence on distance (Fig. 3). In the classical model the geometric mean of c_p/c_o grows from 0.94 at 50 m to 3.26 at 800 m; a constant factor shifts the five arcs together and leaves this trend essentially unchanged (0.80 to 2.28 at $f = 1.35$; 0.63 to 1.53 at $f = 1.9$), whereas with $\alpha = 0.91$ the ratio stays between 0.81 and 1.19 at all five arcs. The fractional order therefore changes the rate at which the ground-level concentration decays with distance, which a constant multiple of the diffusivity does not. This control is also in-sample, and it does not exclude that a classical K_z with a different height dependence could produce the same change.

Table 3 Statistical indices for the convective Prairie Grass experiment (crosswind-integrated ground-level concentration, 20 runs, 100 pairs; this work: Eqs. 3 and 9). Values in brackets are block-bootstrap 95% confidence intervals for the proposed model. *Lagrangian model. †Strongly convective subset ($-h/L > 10$, 19 runs, 95 pairs) of Moreira (2022); on the same subset the proposed model gives $Cor = 0.977$, $NMSE = 0.076$, $FB = -0.154$, $FA2 = 0.726$ at $\alpha = 1$ and 0.978, 0.084, +0.061, 0.947 at $\alpha = 0.91$.

Model	Cor	NMSE	FS	FB	FA2
This work, $\alpha = 1$ (classical limit)	0.978	0.076	+0.137	-0.148	0.720
95% CI	[0.97, 0.99]	[0.05, 0.10]	[+0.10, +0.17]	[−0.18, −0.12]	[0.64, 0.80]
This work, $\alpha = 0.91$	0.975	0.104	+0.224	+0.076	0.940
95% CI	[0.97, 0.98]	[0.06, 0.15]	[+0.16, +0.29]	[+0.04, +0.12]	[0.87, 0.99]
Carvalho et al. (2007)*	0.96	0.10	-0.06	-0.06	0.72
Kumar and Sharan (2012)	0.95	0.22	+0.67	+0.13	0.81
Moreira et al. (2009), ADMM	0.92	0.25	+0.20	+0.03	0.68
Moreira et al. (2009), GILTT	0.90	0.32	+0.33	+0.16	0.72
Moreira (2022), $\alpha = \beta = 1$†	0.98	0.10	—	-0.24	0.70
Moreira (2022), $\beta = 0.64$†	0.99	0.07	—	+0.13	0.96

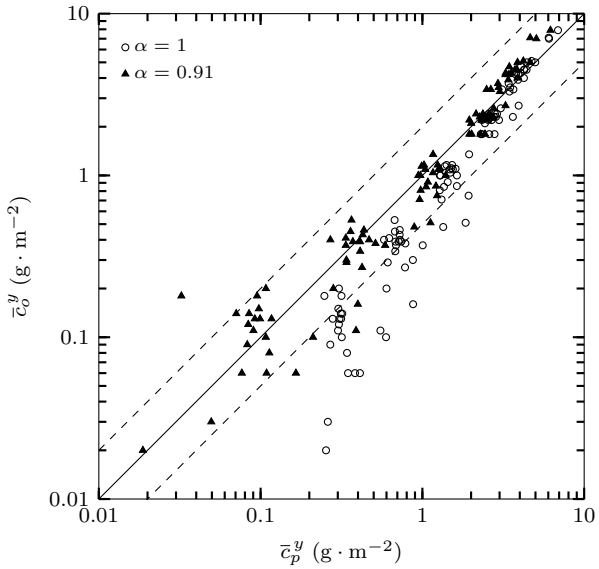


Fig. 2 Predicted versus observed crosswind-integrated ground-level concentrations for the convective Prairie Grass experiment (Eqs. 3 and 9) at $\alpha = 1$ (open circles) and $\alpha = 0.91$ (filled triangles). Solid line: perfect agreement; dashed lines: factor-of-two bounds.

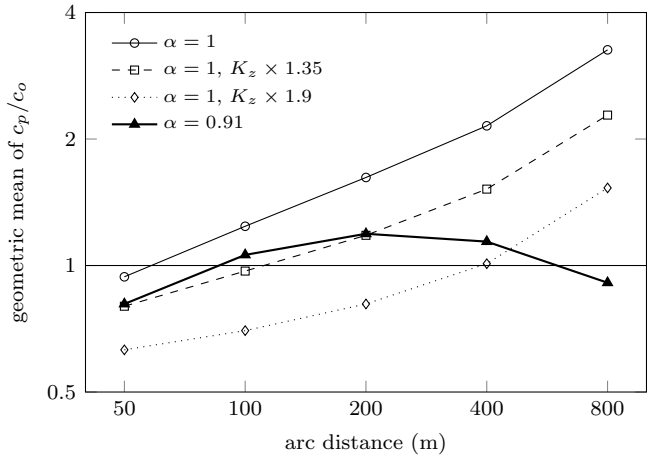


Fig. 3 Convective Prairie Grass (20 runs): geometric mean of the ratio of predicted to observed crosswind-integrated concentration at each arc, for the classical model ($\alpha = 1$), the classical model with K_z multiplied by 1.35 and by 1.9, and the fractional model ($\alpha = 0.91$, original K_z). A constant factor shifts the five arcs together; the fractional order removes the trend with distance.

Table 4 Classical control for convective Prairie Grass (20 runs, 100 pairs, $\overline{c}^{\,y}$): model with $\alpha = 1$ and K_z multiplied by a constant factor f, compared with the model with $\alpha = 0.91$ and the original K_z. Columns 50–800 m: geometric mean of c_p/c_o per arc. Last column: paired difference in FA2 ($\alpha = 0.91$ minus the row), with 95% block-bootstrap interval (10 000 resamples, the experiment as the unit). Reference mesh 640×160.

configuration	NMSE	Cor	FA2	FB	FS	50 m	100 m	200 m	400 m	800 m	paired ΔFA2
$f = 1.00$	0.076	0.978	0.72	−0.15	0.14	0.94	1.24	1.62	2.15	3.26	+0.22 [+0.14; +0.30]
$f = 1.20$	0.077	0.983	0.80	−0.01	0.23	0.85	1.07	1.34	1.74	2.63	+0.14 [+0.06; +0.23]
$f = 1.35$	0.116	0.986	0.84	+0.08	0.30	0.80	0.97	1.18	1.52	2.28	+0.10 [+0.03; +0.17]
$f = 1.50$	0.180	0.987	0.90	+0.17	0.36	0.75	0.88	1.05	1.34	2.02	+0.04 [0.00; +0.09]
$f = 1.70$	0.300	0.987	0.90	+0.27	0.45	0.69	0.78	0.92	1.16	1.74	+0.04 [0.00; +0.09]
$f = 1.90$	0.451	0.986	0.92	+0.37	0.52	0.63	0.70	0.81	1.01	1.53	+0.02 [−0.03; +0.07]
$\alpha = 0.91$, $f = 1$	0.104	0.975	0.94	+0.08	0.22	0.81	1.06	1.19	1.14	0.91	—

5.1.3 Convective regime: Kincaid

Kincaid was simulated with the three-dimensional model — same equations, parameterisations and mesh, with the Briggs plume rise added — and with α fixed beforehand; it is therefore an out-of-sample evaluation. Table 5 and Fig. 4 give the results for the 166 pairs. At $\alpha = 1$ the model satisfies the three acceptance criteria ($|FB| = 0.25$, $NMSE = 0.52$, $FA2 = 0.78$). Its FA2 (0.783, CI [0.70, 0.85]) is the highest among the published evaluations compiled for this campaign (GILTT 0.75, Gaussian 0.74, GIADMT 0.67–0.71), although only the lowest of these values falls outside its confidence interval; the correlation (0.70, CI [0.52, 0.83]) and the NMSE (0.52, CI [0.31, 0.71]) are at the level of the reference models. The fractional bias (−0.25, CI [−0.37, −0.11]) indicates an overprediction that the three Eulerian reference solutions ($|FB| \leq 0.10$) do not show, and FS (−0.46) indicates a predicted distribution wider than the observed one. By arc, the model underestimates at the two nearest arcs (median $c_p/c_o = 0.72$–0.90 at 1–2 km) and overestimates at most arcs from 3 km

onwards (1.1–1.4). An underestimate near the source followed by an overestimate farther downwind is the pattern expected when the plume reaches the ground later in the model than in the atmosphere, as happens when the descent of an elevated plume in convective downdrafts is represented by gradient diffusion, or when the plume rise is overestimated; the question is left open. These comparisons of level indicate that the parameterisations of Section 3, with no adjusted constant, remain competitive for a release type different from those on which α was selected.

The fractional order degrades the Kincaid results significantly on every index except the correlation. At $\alpha = 0.91$ FA2 falls to 0.663 (paired -0.120 $[-0.191; -0.054]$), NMSE rises from 0.52 to 0.86 ($+0.344$ $[+0.171; +0.490]$), the overprediction increases ($FB = -0.48$, paired -0.234 $[-0.246; -0.222]$) and the $|FB|$ criterion is no longer met. For a buoyant plume released at about $0.6\,h$ the material is not carried from the surface by organised updrafts, and a memory anchored at the ground has no physical counterpart. Together with the Prairie Grass results, this indicates that the fractional gain is a property of surface releases in the CBL and not of the operator in general; an adjustment of α per campaign would have concealed this distinction.

The Model Validation Kit provides tower winds for 48 of the 53 experiments. The reference profile reproduces the 10-m wind (median ratio 1.03) and underestimates the 100-m wind by 9%; rescaling it to the measured 100-m wind, with the plume rise recomputed, changes the classical FA2 by two of the 144 pairs with tower data ($0.757 \rightarrow 0.771$; $+0.014$ $[-0.025; +0.054]$) and leaves the effect of the fractional order unchanged (-0.090 $[-0.161; -0.021]$). The reference convention is therefore kept for all data sets.

5.1.4 Stable regime: Prairie Grass

Table 6 presents the indices for the 25 stable Prairie Grass runs (75 pairs), for the 23-run clean set and for the comparison models (scatter diagram in Fig. 5). At $\alpha = 1$ the model meets the NMSE and FA2 criteria (0.78 and 0.69) but not the bias

Table 5 Statistical indices for the Kincaid experiment (arc-maximum concentration normalised by the emission rate, 53 experiments, 166 pairs; this work: Eqs. 6 and 9 with the Briggs plume rise). Values in brackets are block-bootstrap 95% confidence intervals for the proposed model. Literature values as compiled from the cited sources; the number of pairs retained differs among published studies, so these are level comparisons.

Model	Cor	NMSE	FS	FB	FA2
This work, $\alpha = 1$ (classical limit)	0.696	0.516	-0.457	-0.245	0.783
95% CI	[0.52, 0.83]	[0.31, 0.71]	[−0.65, −0.05]	[−0.37, −0.11]	[0.70, 0.85]
This work, $\alpha = 0.91$	0.699	0.859	-0.678	-0.480	0.663
95% CI	[0.53, 0.83]	[0.52, 1.17]	[−0.85, −0.32]	[−0.60, −0.35]	[0.56, 0.76]
GILTT (Buske, 2008)	0.69	0.40	-0.22	+0.05	0.75
Gaussian (Moreira et al., 2004)	0.61	0.54	+0.20	+0.33	0.74
GIADMT, $S_k = 0.6$ (Costa et al., 2006)	0.72	0.47	-0.40	-0.02	0.71
GIADMT, $S_k = 1.0$ (Costa et al., 2006)	0.68	0.43	-0.22	+0.10	0.67

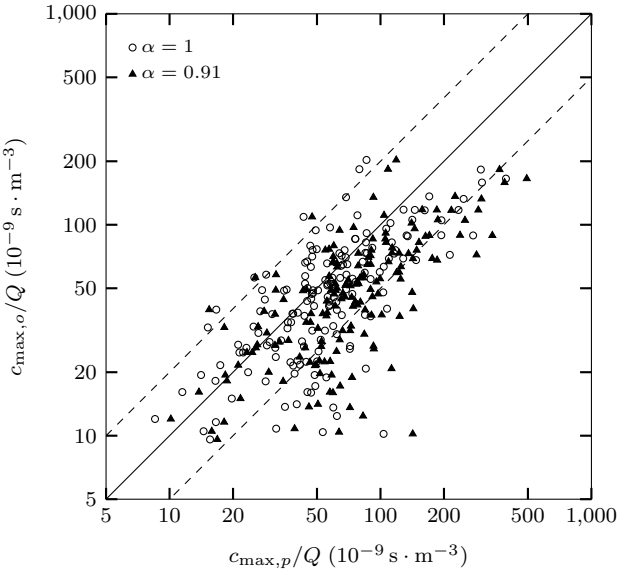


Fig. 4 Predicted versus observed normalised arc-maximum concentrations for the Kincaid experiment (Eqs. 6 and 9, with the Briggs plume rise) at $\alpha = 1$ (open circles) and $\alpha = 0.91$ (filled triangles). Solid line: perfect agreement; dashed lines: factor-of-two bounds.

criterion: $FB = +0.43$ (CI [+0.26, +0.59]), a systematic underprediction of the arc integrals. Removing the two anomalous runs raises the correlation from 0.74 to 0.95 (CI [0.90, 0.98]) — these runs contain the two largest overpredictions of the set (factors of 3.4 and 4.5 at single arcs) — while the underprediction becomes more uniform

($FB = +0.56$) and FA2 remains at 0.70. This is the least favourable comparison with the literature among the five data sets: the correlations of the three reference models (0.71–0.81) and the NMSE and FA2 of Kumar and Sharan (2012) lie inside the confidence intervals of the proposed model, but the NMSE (0.39 and 0.49) and the FA2 (0.95 and 0.82) published for the Lagrangian model of Carvalho et al. (2007) and for the Eulerian model of Moreira et al. (2002) are better, and all three references report overprediction where the present model underpredicts. Two observations qualify this comparison. First, the deficit is concentrated at the nearest arc: at 50 m the model recovers 0.48 of the observed $\overline{c}^{y}$ in the median, whereas at 200 and 800 m the arc integrals, lateral widths and arc maxima are within 0.8–1.0 of the observations (Section 5.4, Fig. 8). Second, the tabulated "U_{10}" of the stable runs, commonly used as the reference wind for this data set, is 20% below the 10-m mast wind (Section 3.4); rescaling the present model to that wind would raise its classical FA2 to 0.89, but with a transport wind lower than the measured one (Section 5.3).

The fractional order does not improve the results in the stable surface layer. At $\alpha = 0.91$ FA2 falls to 0.56 (paired -0.133 $[-0.240; -0.040]$; -0.116 $[-0.217; -0.043]$ on the clean set), NMSE rises from 0.78 to 1.05 ($+0.268$ $[+0.086; +0.433]$) and the underprediction increases ($FB = +0.57$; paired $+0.133$ $[+0.109; +0.156]$), while the correlation is unchanged. Under stable stratification vertical motions are suppressed, and there is no physical basis for ground-anchored non-local transport.

5.1.5 Stable regime: Hanford 83

Table 7 reports the comparison between the proposed model and the analytical model of Kumar and Sharan (2010) for the Hanford 83 experiment (scatter diagram in Fig. 6). The model satisfies all three acceptance criteria at both orders ($|FB| = 0.12$ and 0.01, $NMSE = 0.26$ and 0.28, $FA2 = 0.70$ and 0.83). With six experiments the confidence intervals are broad (FA2 [0.33, 1.00] at $\alpha = 1$), and every published index of the Kumar–Sharan model — $Cor = 0.91$, $NMSE = 0.21$, $FS = +0.12$, $FB = -0.14$,

Table 6 Statistical indices for the stable Prairie Grass experiment (crosswind-integrated ground-level concentration, 25 runs, 75 pairs, and the clean set of 23 runs without runs 13 and 14; this work: Eqs. 3 and 8). Values in brackets are block-bootstrap 95% confidence intervals for the proposed model. *Lagrangian model.

Model	Cor	NMSE	FS	FB	FA2
This work, $\alpha = 1$ (classical limit)	0.742	0.783	+0.386	+0.434	0.693
95% CI	[0.66, 0.97]	[0.64, 0.93]	[+0.12, +0.77]	[+0.26, +0.59]	[0.61, 0.77]
This work, $\alpha = 0.91$	0.734	1.052	+0.451	+0.566	0.560
95% CI	[0.66, 0.97]	[0.75, 1.36]	[+0.17, +0.87]	[+0.37, +0.74]	[0.44, 0.67]
clean set (69 pairs), $\alpha = 1$	0.950	0.833	+0.747	+0.563	0.696
95% CI	[0.90, 0.98]	[0.67, 0.98]	[+0.67, +0.82]	[+0.47, +0.63]	[0.61, 0.78]
clean set (69 pairs), $\alpha = 0.91$	0.957	1.240	+0.842	+0.714	0.580
95% CI	[0.91, 0.98]	[1.02, 1.43]	[+0.77, +0.91]	[+0.63, +0.78]	[0.46, 0.70]
Kumar and Sharan (2012)	0.71	0.72	-1.05	-0.57	0.68
Moreira et al. (2002)	0.77	0.49	-0.26	-0.22	0.82
Carvalho et al. (2007)*	0.81	0.39	-0.18	-0.06	0.95

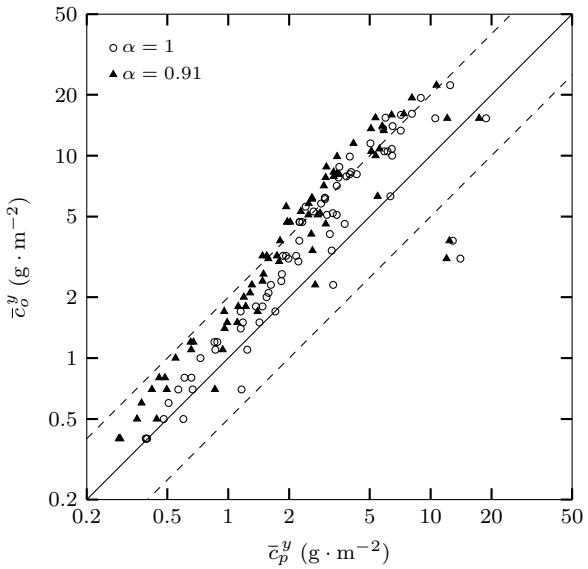


Fig. 5 Predicted versus observed crosswind-integrated ground-level concentrations for the stable Prairie Grass experiment at $\alpha = 1$ (open circles) and $\alpha = 0.91$ (filled triangles). Solid line: perfect agreement; dashed lines: factor-of-two bounds.

$FA2 = 0.73$ — lies within the corresponding interval of the proposed model, so the two formulations must be regarded as statistically indistinguishable on this campaign. The fractional order moves the point values in the favourable direction — the FA2 rises from 0.70 to 0.83 and the mild overprediction of the classical limit ($FB = -0.12$) is removed

(−0.01) — but only the change in bias is significant (+0.107 [+0.096; +0.112]); the paired change in FA2 (+0.133 [+0.000; +0.333]) does not exclude zero, and the NMSE and the correlation are unchanged. With six experiments, the Hanford 83 data do not discriminate the fractional order.

Table 7 Statistical indices for the Hanford 83 experiment (crosswind-integrated ground-level concentration normalised by the emission rate, 6 runs, 30 pairs; this work: Eqs. 3 and 8). Values in brackets are block-bootstrap 95% confidence intervals for the proposed model.

Model	Cor	NMSE	FS	FB	FA2
This work, $\alpha = 1$ (classical limit)	0.880	0.262	+0.189	-0.115	0.700
95% CI	[0.77, 0.96]	[0.09, 0.62]	[−0.14, +0.43]	[−0.46, +0.14]	[0.33, 1.00]
This work, $\alpha = 0.91$	0.881	0.281	+0.231	-0.008	0.833
95% CI	[0.77, 0.96]	[0.08, 0.61]	[−0.09, +0.46]	[−0.36, +0.25]	[0.57, 1.00]
Kumar and Sharan (2010)	0.91	0.21	+0.12	-0.14	0.73

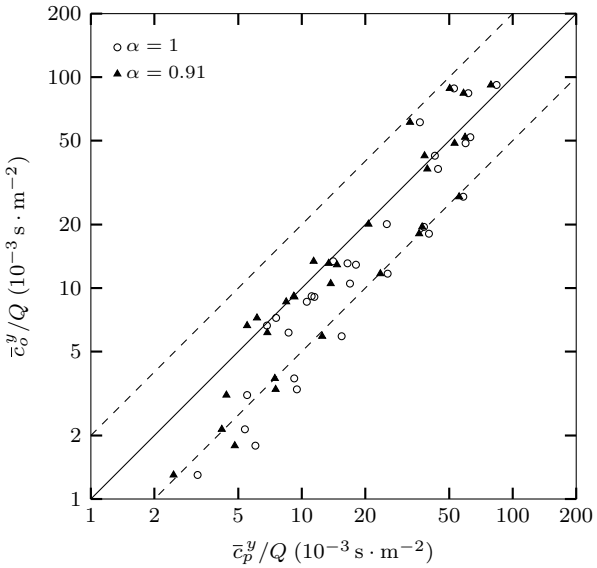


Fig. 6 Predicted versus observed normalised crosswind-integrated ground-level concentrations for the Hanford 83 experiment at $\alpha = 1$ (open circles) and $\alpha = 0.91$ (filled triangles). Solid line: perfect agreement; dashed lines: factor-of-two bounds.

5.2 Arc-maximum concentrations: the three-dimensional model

The comparisons of Section 5.1 for the four classical data sets use the crosswind-integrated concentration, on which the fractional order was selected. The three-dimensional model of Eq. (6) predicts the arc-maximum concentration, which also depends on the lateral closure and was not used to select α. It is not statistically independent of $\overline{c}^{\,y}$, since both are measured in the same runs, but it tests the same order on a different observable. Table 8 reports the five indices with their confidence intervals for the three data sets with tabulated arc maxima (193 pairs; scatter diagrams in Fig. 7). The median ratio between the modelled and the observed lateral widths, $\sigma_y = \overline{c}^{\,y}/(\sqrt{2\pi}\, c_{\max})$, is 1.08 for Copenhagen, 1.03 for convective Prairie Grass and 0.76 for the stable set at $\alpha = 1$, and 0.99, 0.84 and 0.96 at $\alpha = 0.91$.

The convective gain persists in this observable: for convective Prairie Grass FA2 increases from 0.695 ($\alpha = 1$) to 0.832 ($\alpha = 0.91$), a paired +0.137 [+0.053; +0.232], and the correlation from 0.89 to 0.92 (+0.031 [+0.008; +0.053]), while NMSE is unchanged within its interval. The arc maxima, however, become overpredicted (FB −0.10 → −0.30, at the limit of the acceptance criterion) because the modelled plume narrows (width ratio 1.03 → 0.84): part of the vertical gain is offset by the lateral closure. Copenhagen is again saturated ($FA2 = 0.957$ at both orders, 22 of 23 pairs). The stable set again favours $\alpha = 1$: on the clean set $FA2 = 0.928$, $Cor = 0.957$ and $NMSE = 0.38$ at $\alpha = 1$, against 0.797, 0.952 and 0.97 at $\alpha = 0.91$ (paired −0.130 [−0.246; −0.029] in FA2), with FB increasing from +0.29 to +0.52; the full 75-pair set, whose correlation (0.64) is dominated by the two anomalous runs, shows the same loss. Pooled over the 193 pairs the gain is not significant (+0.037 [−0.005; +0.081] at $\alpha = 0.93$). In three dimensions, therefore, only the gain for convective surface releases is statistically supported.

Table 8 Statistical indices of the three-dimensional model (Eq. 6) for the arc-maximum concentration at the sampling height, with block-bootstrap 95% confidence intervals (in brackets, below each row). Copenhagen: $c_{\max}/Q$; Prairie Grass: $c_{\max}$ at 1.5 m.

Campaign (pairs)	α	Cor	NMSE	FS	FB	FA2
Copenhagen, $c_{\max}/Q$ (23)	1	0.821	0.216	-0.014	+0.108	0.957
		[0.74, 0.97]	[0.10, 0.30]	[−0.36, +0.55]	[−0.13, +0.34]	[0.87, 1.00]
	0.91	0.843	0.183	-0.084	+0.030	0.957
		[0.78, 0.98]	[0.05, 0.30]	[−0.45, +0.36]	[−0.19, +0.23]	[0.87, 1.00]
PG convective, $c_{\max}$ (95)	1	0.893	0.436	+0.026	-0.102	0.695
		[0.82, 0.97]	[0.14, 0.79]	[−0.18, +0.23]	[−0.27, +0.07]	[0.57, 0.80]
	0.91	0.924	0.479	-0.197	-0.301	0.832
		[0.87, 0.98]	[0.26, 0.77]	[−0.37, −0.02]	[−0.44, −0.16]	[0.69, 0.94]
PG stable, $c_{\max}$ (75)	1	0.635	1.667	-0.329	-0.065	0.880
		[0.53, 0.97]	[0.27, 2.67]	[−0.69, +0.35]	[−0.43, +0.33]	[0.76, 0.97]
	0.91	0.655	1.394	-0.043	+0.210	0.760
		[0.54, 0.97]	[0.79, 1.81]	[−0.42, +0.59]	[−0.14, +0.56]	[0.61, 0.89]
clean set (69)	1	0.957	0.383	+0.309	+0.290	0.928
		[0.92, 0.99]	[0.16, 0.69]	[+0.20, +0.43]	[+0.18, +0.41]	[0.83, 1.00]
	0.91	0.952	0.967	+0.550	+0.519	0.797
		[0.91, 0.98]	[0.59, 1.39]	[+0.45, +0.65]	[+0.40, +0.63]	[0.65, 0.93]

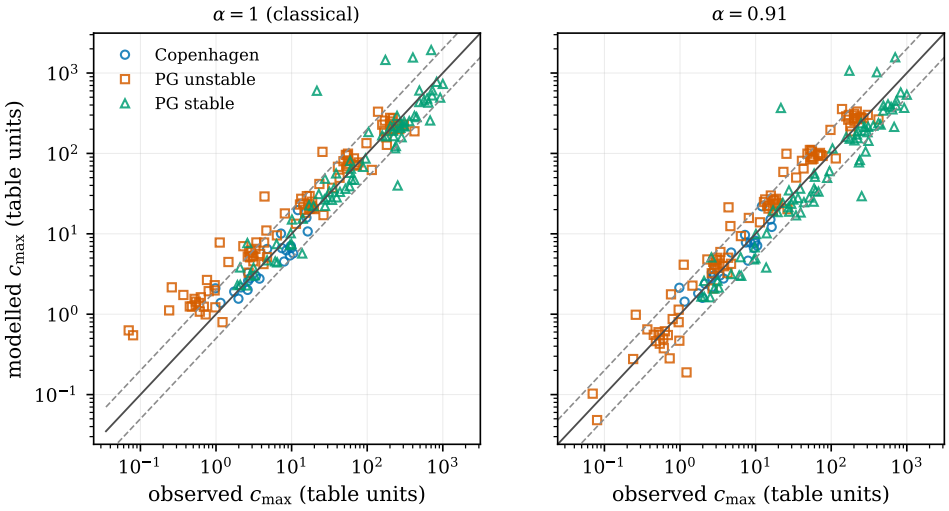


Fig. 7 Observed versus modelled arc-maximum concentration for the three campaigns with tabulated maxima (each in its table units), at $\alpha = 1$ (left) and $\alpha = 0.91$ (right). Solid line: perfect agreement; dashed: factor of two.

5.3 Sensitivity to the wind-profile convention

Eulerian dispersion models differ in their treatment of the wind profile: some retain the tabulated u_* (as here), others rescale a similarity or power-law profile to a tabulated

reference wind, and most hold the wind constant above a cutoff height. Since the transport wind affects every predicted concentration, the effect of each convention on the results of Section 5.1 was quantified with everything else unchanged and with the same paired block bootstrap (Table 9). Four variants were run: the reference profile without the cutoff (*uncut*); the reference shape rescaled to the tabulated reference wind (*anchored*: U_{10} at Prairie Grass and Copenhagen, U_2 at Hanford), which is the convention of the models tied to an anemometer (Gonçalves et al., 2013; Moreira, 2022); the same anchoring without the cutoff; and, for Copenhagen only, anchoring at the 115-m release height instead of 10 m.

Table 9 Sensitivity to the wind-profile convention (2-D, $\overline{c}^{\,y}$). Mast: median ratio of the model wind to the Prairie Grass mast wind over all levels 0.5–16 m (convective runs / clean stable runs). $\mathrm{FA2}_{\alpha=1}$: stable Prairie Grass (75 pairs) / Hanford 83 (30) / pooled (228). Gain: paired difference $\alpha = 0.91$ minus $\alpha = 1$ within each convention, pooled and for the two Prairie Grass sets, with 95% block-bootstrap intervals; $\star$ marks intervals excluding zero. Copenhagen saturates at 1.000 and convective Prairie Grass moves by at most one pair in every variant; Kincaid is examined against its measured 100-m wind in Section 5.1.

convention	mast conv. / stab.	$\mathrm{FA2}_{\alpha=1}$ PGs / Han / pooled	gain, pooled $\alpha = 0.91$	gain, PGu / PGs $\alpha = 0.91$
reference (cut)	0.97 / 0.92	0.693 / 0.700 / 0.737	$+0.070^{\star}$ $[+0.02; +0.12]$	$+0.22^{\star}$ / $-0.13^{\star}$
uncut	0.97 / 0.92	0.693 / 0.700 / 0.737	$+0.066^{\star}$ $[+0.01; +0.12]$	$+0.22^{\star}$ / $-0.15^{\star}$
anchored, cut	0.99 / 0.80	0.787 / 0.600 / 0.750	$+0.040$ $[-0.00; +0.08]$	$+0.23^{\star}$ / $-0.23^{\star}$
anchored, uncut	0.99 / 0.80	0.893 / 0.633 / 0.789	$+0.027$ $[-0.02; +0.07]$	$+0.23^{\star}$ / $-0.25^{\star}$

Three results follow. First, the cutoff has no effect on the indices: removing it changes no FA2 at $\alpha = 1$ and changes the values at $\alpha = 0.91$ by one pair in the stable sets, because the plume remains below z_b in the cases concerned. Measured profiles nevertheless contradict the cutoff: with it, the model wind at 16 m is 0.43–0.46 of the Prairie Grass mast wind in the most stable runs (0.94 without it), and tower winds from Hanford 67 (Nickola, 1977) agree with the uncut profile (median ratio

0.997 at 15.2 m). The cutoff is kept for consistency with the earlier models and has no consequence for the conclusions. Second, anchoring to the tabulated stable winds raises the classical stable Prairie Grass FA2 from 0.693 to 0.893 (+0.20 [+0.13; +0.27], anchored uncut; +0.09 [−0.01; +0.19] with the cutoff) and the pooled classical baseline from 0.737 to 0.789 (+0.05 [+0.03; +0.08]). This is not a physical improvement: the anchored wind is 20% *below* the mast wind at every level (ratio 0.80, against 0.92 for the reference), so the higher score results from a transport wind that is too low, which compensates the 20–30% underestimate at the 200- and 800-m arcs; it also changes the Hanford 83 FA2 by −0.10 [−0.17; −0.03]. The reference convention is therefore kept. Third, the pooled fractional gain depends on the convention. Under the reference and uncut profiles it is significant (+0.070 and +0.066 at $\alpha = 0.91$; +0.053 at 0.93); under the anchored conventions it is not (+0.040 [−0.004; +0.083] and +0.027 [−0.018; +0.070]), because the anchored stable baseline starts higher and loses more for $\alpha < 1$ (−0.23 to −0.25, against −0.13). The partition by regime, in contrast, does not depend on the convention: the gain for convective surface releases is +0.22 to +0.23, and the stable loss is significant, in all four variants. The robust result is thus a large gain for convective surface releases and a loss in stable conditions; the sign of their pooled balance depends on the wind convention. Finally, anchoring Copenhagen at the wind measured at the release height (of which the profile gives 0.79) leaves FA2 at 1.000 and doubles NMSE (0.06 → 0.13; FB +0.05 → +0.19): the deficit of the profile above the surface layer does not affect the conclusions for that campaign.

5.4 Limitations of the proposed model

The main limitations identified in this study are the following.

The 50-m arc of stable Prairie Grass

The systematic residual on the clean stable set is concentrated at the nearest arc (Fig. 8): at 50 m the model recovers 0.48 of the observed $\bar{c}^{\,y}$ in the median and its σ_y

is 0.66 of the observed, whereas at 200 and 800 m all three quantities are within 0.8–1.0. Two distinct deficits are involved. The first is lateral. Inverting Taylor's theorem per run with σ_v free shows that the observed widths require $\sigma_v^2 = (2.2\,u_*)^2 + \sigma_{\mathrm{meso}}^2$: a mechanical turbulent part plus an additive term $\sigma_{\mathrm{meso}} \approx 0.3$–$0.7$ m s^{-1} that does not scale with u_* and correlates with neither $1/L$ nor U_{10}, as expected of submeso motions (Mahrt, 2009); with $U_{10} = 2.8$–7.7 m s^{-1} in these runs it corresponds to wind-direction fluctuations of 5–9°. This additional variance explains the narrow modelled plume, but not the deficit in $\overline{c}^{\,y}$, which does not depend on the lateral closure; for the same reason the meander interpolation of AERMOD (Cimorelli et al., 2005), which conserves $\overline{c}^{\,y}$ by construction, does not remove it. The second deficit is in $\overline{c}^{\,y}$ itself: at 50 m the observed value exceeds the maximum attainable under the measured wind for any vertical spread, $\max_{\sigma_z} \overline{c}^{\,y}(\sigma_z)$, in 22 of the 23 clean runs, so that no vertical diffusivity can reproduce this arc. Its origin remains unidentified. Since the additional lateral variance cannot be parameterised from the local variables available to the model, and a fitted lower bound on σ_v raises the 50-m arc maxima but degrades the other two arcs, both deficits are recorded as limitations.

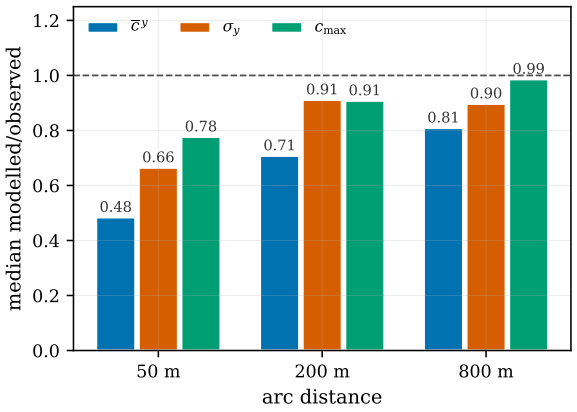


Fig. 8 Stable Prairie Grass, clean set (23 runs), $\alpha = 1$: median modelled/observed ratio per arc for the crosswind-integrated concentration, the lateral width, and the arc maximum. The deficit is concentrated at the 50-m arc and is largest in $\overline{c}^{\,y}$.

Selection of the order and other simplifications

The order was selected on the four classical data sets, so the indices reported for them at $\alpha < 1$ are in-sample; the gain originates in a single data set (convective Prairie Grass, 20 runs), and its confirmation requires independent surface-release experiments in convective conditions; the classical control of Section 5.1 was run on the same data. The operating value lies slightly below the positivity bound of the reference mesh (Section 2.2). The model assumes stationarity and horizontal homogeneity, a strong idealisation for the Kincaid arcs at tens of kilometres, and neglects deposition, which may affect the SO_2 tracer of Prairie Grass at the farthest arcs.

Non-transferability of the fractional order

The numerical value of a fractional order is not transferable between operator placements. For these same campaigns, published orders range from 0.54 to 0.99 according to whether the operator is in the advective term (Acioli et al., 2019; Goulart et al., 2017), in the concentration flux (Goulart et al., 2019), in both, or is a local deformed derivative (Goulart et al., 2020); and the behaviour by regime changes with the operator: the model of Goulart et al. (2019), with fractional orders in both the advective term and the flux, *improves* stable Prairie Grass, where the present formulation loses skill, through the slowly decaying Mittag–Leffler tail of the fractional advection, which Eq. (3) does not contain. The value $\alpha = 0.91$ is therefore specific to the present operator. Classical closures with distance-dependent diffusivities can also reach comparable skill for convective surface releases (Acioli et al., 2019); the fractional formulation reaches it with distance-independent parameterisations taken from the literature.

6 Conclusions

An Eulerian dispersion model was formulated in which the vertical turbulent flux of the advection–diffusion equation is written with a Caputo fractional derivative of

a single order α and, in three dimensions, the lateral flux with a symmetric Riesz operator. The model was evaluated against five field data sets with five statistical indices per data set, block-bootstrap 95% confidence intervals with the experiment as the resampling unit, paired differences between configurations, published acceptance criteria and the published indices of established models.

The main conclusions are as follows. (i) In the classical limit the model meets the acceptance criteria of Hanna and Chang (2012) ($|FB| \leq 0.30$, $NMSE \leq 3$, $FA2 \geq 0.5$) for Copenhagen, convective Prairie Grass, Hanford 83 and Kincaid, and two of the three for stable Prairie Grass, where the arc integrals are underpredicted ($FB = +0.43$), mainly at the 50-m arc. (ii) For most indices the classical limit is statistically indistinguishable from the Eulerian, semi-analytical and Lagrangian reference models for Copenhagen and Hanford 83; for Kincaid its FA2 (0.78) is at the level of the published values, with a larger overprediction ($FB = -0.25$); for stable Prairie Grass the two best reference models have better NMSE and FA2. (iii) A single order $\alpha = 0.91$ raises the FA2 of the convective Prairie Grass runs from 0.72 to 0.94 (paired gain $+0.22$ $[+0.14; +0.30]$) and reduces the magnitude of their bias, at the cost of a slightly higher NMSE; the gain is consistent with that of the two-order fractional model of Moreira (2022) on the same runs and persists in the arc-maximum concentrations ($+0.14$ $[+0.05; +0.23]$). A constant rescaling of the classical K_z recovers most of the gain in FA2 (up to 0.90–0.92) only with a bias of opposite sign and a larger NMSE, and leaves the growth of the classical residuals with distance (a factor of about three between 50 and 800 m), which the fractional order removes. The same order leaves Copenhagen and Hanford 83 statistically unchanged and degrades stable Prairie Grass (-0.13 in FA2) and Kincaid (-0.12). (iv) The benefit of the fractional operator is therefore restricted to surface releases in the convective boundary layer, where non-local vertical transport by organised thermals is expected; it is not a general property

of the operator, and the sign of the gain pooled over all data sets depends on the wind-profile convention.

The limitations are the underprediction at the nearest arc of stable Prairie Grass, which no vertical diffusivity can remove; the loss of skill for $\alpha < 1$ in stable conditions and for the elevated buoyant release; the residual pattern with distance at Kincaid; the surface-layer wind profile and its cutoff, which measured profiles contradict without consequence for the results; the mesh dependence of the usable range of α; and the selection of the order on the four classical data sets, only partly offset by the out-of-sample evaluation on Kincaid. Future work should address the determination of the fractional order from measured turbulence statistics rather than from concentrations, the representation of elevated releases in the convective boundary layer, and the evaluation against independent surface-release data, including paired significance tests between models as recommended by Chang and Hanna (2004).

Supplementary information

Online Resource 1 lists the meteorological data of the field experiments used to drive the model (Table S1 to Table S5).

Acknowledgements

The authors thank the Conselho Nacional de Desenvolvimento Científico e Tecnológico (CNPq, Brazil) for financial support (process 403000/2023-8).

Declarations

- **Funding.** This work was supported by the Conselho Nacional de Desenvolvimento Científico e Tecnológico (CNPq, Brazil), process 403000/2023-8.
- **Competing interests.** The authors have no relevant financial or non-financial interests to disclose.

- **Ethics approval and consent to participate.** Not applicable.
- **Author contributions.** All authors contributed equally to this work.
- **Data availability.** The field data sets used in this study are published in the sources cited in Section 4.1; the compiled data sets with their quality-control scripts will be made available in a public repository upon publication.
- **Code availability.** The model code and the scripts that reproduce every table and figure of this paper will be made available in the same public repository upon publication.
- **Use of artificial intelligence.** A large language model (Claude, Anthropic) was used as described at the end of Section 4.2; the authors reviewed the output and take full responsibility for the content of this article.
- **ORCID.** Antonio Goulart: https://orcid.org/0000-0002-7228-5805, Julian M. S. Suarez: https://orcid.org/0000-0002-0788-9979, Joice C. Marques: https://orcid.org/0000-0003-2137-2164, Adelaida O. Conza: https://orcid.org/0000-0003-4793-0400, Matheus J. Lazo: https://orcid.org/0000-0001-9741-9411.

References

Acioli, P.S., Xavier, F.A., Moreira, D.M. (2019). Mathematical model using fractional derivatives applied to the dispersion of pollutants in the planetary boundary layer. *Boundary-Layer Meteorology*, *170*(2), 285–304, https://doi.org/10.1007/s10546-018-0403-1

Baeumer, B., Kovács, M., Meerschaert, M.M., Sankaranarayanan, H. (2018). Boundary conditions for fractional diffusion. *Journal of Computational and Applied Mathematics*, *336*, 408–424, https://doi.org/10.1016/j.cam.2017.12.053

748 Barad, M.L. (Ed.). (1958). *Project Prairie Grass, a field program in diffusion*. Bedford,
749 MA: Air Force Cambridge Research Center. (Mast wind and temperature profiles
750 (Vol. I, Table 8.1) as digitised by J. S. Irwin, https://www.harmo.org/jsirwin/
751 PGrassTTUU.txt)

752 Benson, D.A., Wheatcraft, S.W., Meerschaert, M.M. (2000). Application of a
753 fractional advection-dispersion equation. *Water Resources Research*, *36*(6),
754 1403–1412, https://doi.org/10.1029/2000WR900031

755

756 Bowne, N.E., & Londergan, R.J. (1983). *Overview, results and conclusions for the*
757 *EPRI plume model validation and development project: plains site* (Tech. Rep.
758 No. EPRI Report EA-3074). Palo Alto, CA: Electric Power Research Institute.

759 Briggs, G.A. (1975). Plume rise predictions. *Lectures on air pollution and envi-*
760 *ronmental impact analyses* (pp. 59–111). Boston: American Meteorological
761 Society.

762 Businger, J.A., Wyngaard, J.C., Izumi, Y., Bradley, E.F. (1971). Flux-profile rela-
763 tionships in the atmospheric surface layer. *Journal of the Atmospheric Sciences*,
764 *28*, 181–189,

765

766 Buske, D. (2008). *Solução GILTT bidimensional em geometria cartesiana: simulação*
767 *da dispersão de poluentes na atmosfera* (Unpublished doctoral dissertation).
768 Universidade Federal do Rio Grande do Sul, PROMEC, Porto Alegre.

769 Carvalho, J.C., Vilhena, M.T.M.B., Thompson, M. (2007). An iterative Langevin
770 solution for turbulent dispersion in the atmosphere. *Journal of Computational*
771 *and Applied Mathematics*, *206*, 534–548,

772

773 Chang, J.C., & Hanna, S.R. (2004). Air quality model performance evaluation.
774 *Meteorology and Atmospheric Physics*, *87*, 167–196,
775
776 Cimorelli, A.J., Perry, S.G., Venkatram, A., Weil, J.C., Paine, R.J., Wilson, R.B., ...
777 Brode, R.W. (2005). AERMOD: a dispersion model for industrial source appli-
778 cations. Part I: general model formulation and boundary layer characterization.
779 *Journal of Applied Meteorology*, *44*, 682–693,
780
781 Costa, C.P., Vilhena, M.T., Moreira, D.M., Tirabassi, T. (2006). Semi-analytical
782 solution of the steady three-dimensional advection-diffusion equation in the
783 planetary boundary layer. *Atmospheric Environment*, *40*, 5659–5669,
784
785 Deardorff, J.W. (1966). The counter-gradient heat flux in the lower atmosphere
786 and in the laboratory. *Journal of the Atmospheric Sciences*, *23*(5), 503–506,
787 https://doi.org/10.1175/1520-0469(1966)023⟨0503:TCGHFI⟩2.0.CO;2
788
789 Degrazia, G.A., Anfossi, D., Carvalho, J.C., Mangia, C., Tirabassi, T., Campos Velho,
790 H.F. (2000). Turbulence parameterisation for PBL dispersion models in all
791 stability conditions. *Atmospheric Environment*, *34*, 3575–3583,
792
793 Degrazia, G.A., Campos Velho, H.F., Carvalho, J.C. (1997). Nonlocal exchange
794 coefficients for the convective boundary layer derived from spectral properties.
795 *Contributions to Atmospheric Physics*, *70*, 57–64,
796

797 Degrazia, G.A., & Moraes, O.L.L. (1992). A model for eddy diffusivity in a stable
798 boundary layer. *Boundary-Layer Meteorology*, *58*, 205–214,
799
800 Doran, J.C., & Horst, T.W. (1985). An evaluation of Gaussian plume-depletion models
801 with dual-tracer field measurements. *Atmospheric Environment*, *19*, 939–951,
802
803 Efron, B. (1987). Better bootstrap confidence intervals. *Journal of the American*
804 *Statistical Association*, *82*, 171–185,
805
806 Gonçalves, G.A., Quadros, R., Buske, D. (2013). An analytical formulation for pol-
807 lutant dispersion simulation in the atmospheric boundary layer. *Journal of*
808 *Environmental Protection*, *4*, 57–64,
809
810 Goulart, A., Lazo, M.J., Suarez, J.M.S. (2019). A new parameterization for the
811 concentration flux using the fractional calculus to model the dispersion of con-
812 taminants in the planetary boundary layer. *Physica A*, *518*, 38–49, https://
813 doi.org/10.1016/j.physa.2018.11.064
814
815 Goulart, A., Lazo, M.J., Suarez, J.M.S. (2020). A deformed derivative model for
816 turbulent diffusion of contaminants in the atmosphere. *Physica A*, *557*, 124847,
817 https://doi.org/10.1016/j.physa.2020.124847
818
819 Goulart, A., Lazo, M.J., Suarez, J.M.S., Moreira, D.M. (2017). Fractional derivative
820 models for atmospheric dispersion of pollutants. *Physica A*, *477*, 9–19,
821

822 Gryning, S.-E., & Lyck, E. (1984). Atmospheric dispersion from elevated sources in
823 an urban area: comparison between tracer experiments and model calculations.
824 *Journal of Climate and Applied Meteorology*, *23*, 651–660,
825
826 Hanna, S.R. (1989). Confidence limits for air quality model evaluations, as estimated
827 by bootstrap and jackknife resampling methods. *Atmospheric Environment*, *23*,
828 1385–1398,
829
830 Hanna, S.R., & Chang, J.C. (2012). Acceptance criteria for urban dispersion model
831 evaluation. *Meteorology and Atmospheric Physics*, *116*(3), 133–146,
832
833 Holtslag, A.A.M., & Moeng, C.-H. (1991). Eddy diffusivity and countergradient
834 transport in the convective atmospheric boundary layer. *Journal of the Atmo-*
835 *spheric Sciences*, *48*(14), 1690–1698, https://doi.org/10.1175/1520-0469(1991)
836 048⟨1690:EDACTI⟩2.0.CO;2
837
838 Kelly, J.F., Sankaranarayanan, H., Meerschaert, M.M. (2019). Boundary conditions
839 for two-sided fractional diffusion. *Journal of Computational Physics*, *376*, 1089–
840 1107, https://doi.org/10.1016/j.jcp.2018.10.010
841
842 Kong, M., & Fu, H. (2024). A fast fractional block-centered finite difference method
843 for two-sided space-fractional diffusion equations on general nonuniform grids.
844 *Fractional Calculus and Applied Analysis*, *27*(6), 3446–3476, https://doi.org/
845 10.1007/s13540-024-00346-5
846

Kopteva, N. (2019). Error analysis of the L1 method on graded and uniform meshes for a fractional-derivative problem in two and three dimensions. *Mathematics of Computation*, *88*(319), 2135–2155, https://doi.org/10.1090/mcom/3410

Kumar, P., & Sharan, M. (2010). An analytical model for dispersion of pollutants from a continuous source in the atmospheric boundary layer. *Proceedings of the Royal Society A*, *466*, 383–406,

Kumar, P., & Sharan, M. (2012). Parameterization of the eddy diffusivity in a dispersion model over homogeneous terrain in the atmospheric boundary layer. *Atmospheric Research*, *106*, 30–43,

Lin, Y., & Xu, C. (2007). Finite difference/spectral approximations for the time-fractional diffusion equation. *Journal of Computational Physics*, *225*(2), 1533–1552, https://doi.org/10.1016/j.jcp.2007.02.001

Madiyarov, M., Alimbekova, N., Bakishev, A., Mukhamediyev, G., Yergaliyev, Y. (2025). Nonlocal modeling and inverse parameter estimation of time-varying vehicular emissions in urban pollution dynamics. *Mathematics*, *13*(17), 2772, https://doi.org/10.3390/math13172772

Mahrt, L. (2009). Characteristics of submeso winds in the stable boundary layer. *Boundary-Layer Meteorology*, *130*, 1–14,

Mangia, C., Moreira, D.M., Schipa, I., Degrazia, G.A., Tirabassi, T., Rizza, U. (2002). Evaluation of a new eddy diffusivity parameterisation from turbulent Eulerian spectra in different stability conditions. *Atmospheric Environment*, *36*, 67–76,

Meerschaert, M.M., & Tadjeran, C. (2004). Finite difference approximations for fractional advection–dispersion flow equations. *Journal of Computational and Applied Mathematics*, *172*(1), 65–77, https://doi.org/10.1016/j.cam.2004.01.033

Mooney, C.J., & Wilson, J.D. (1993). Disagreements between gradient-diffusion and Lagrangian stochastic dispersion models, even for sources near the ground. *Boundary-Layer Meteorology*, *64*, 291–296,

Moreira, D.M. (2022). An approach for the atmospheric pollutant dispersion equation considering anomalous diffusion in strongly unstable conditions. *Pure and Applied Geophysics*, *179*, 1433–1443,

Moreira, D.M., Carvalho, J.C., Goulart, A. (2002). A comparison of two turbulent dispersion parameterization in the stable boundary layer by using Lagrangian and Eulerian models. *Revista Brasileira de Geofísica*, *20*(2), 103–112,

Moreira, D.M., & Moret, M. (2018). A new direction in the atmospheric pollutant dispersion inside the planetary boundary layer. *Journal of Applied Meteorology and Climatology*, *57*, 185–192,

Moreira, D.M., Santos, D.P., Carvalho, J.C., Vilhena, M.T., Degrazia, G.A., Tirabassi, T. (2004). A solution of the steady K-diffusion equation for ABL dispersion in inhomogeneous turbulence with plume rise. *Revista Brasileira de Meteorologia*, *19*, 113–122,

Moreira, D.M., Tirabassi, T., Carvalho, J.C. (2005). Plume dispersion simulation in low wind conditions in stable and convective boundary layers. *Atmospheric Environment*, *39*, 3643–3650,

Moreira, D.M., Vilhena, M.T., Buske, D., Tirabassi, T. (2009). The state-of-art of the GILTT method to simulate pollutant dispersion in the atmosphere. *Atmospheric Research*, *92*, 1–17,

Moreira, D.M., Xavier, P., Palmeira, A., Nascimento, E. (2019). New approach to solving the atmospheric pollutant dispersion equation using fractional derivatives. *International Journal of Heat and Mass Transfer*, *144*, 118667,

Nickola, P.W. (1977). *The Hanford 67-series: a volume of atmospheric field diffusion measurements* (Tech. Rep. No. PNL-2433). Richland, WA: Pacific Northwest Laboratory.

Olesen, H.R. (2005). *User's guide to the Model Validation Kit* (Tech. Rep. No. Research Notes from NERI No. 226). Roskilde, Denmark: National Environmental Research Institute. (Kincaid, Copenhagen, Lillestrøm and Indianapolis data sets; https://www.harmo.org/kit/)

Panofsky, H.A., & Dutton, J.A. (1984). *Atmospheric turbulence: Models and methods for engineering applications*. New York: John Wiley & Sons.

Pasquill, F. (1974). *Atmospheric diffusion.* New York: Halstead–Press–Willey.

Paulson, C.A. (1970). The mathematical representation of wind speed and temperature profiles in the unstable atmospheric surface layer. *Journal of Applied Meteorology*, *9*, 857–861,

Prates, J.H.S., Silva, J.R.D., Souza, F.M., Moreira, D.M. (2022). Three-dimensional analytical solution of the fractional atmospheric pollutant dispersion equation considering Caputo and conformable derivatives. *Pure and Applied Geophysics*, *179*(9), 3411–3426, https://doi.org/10.1007/s00024-022-03114-9

Schumer, R., Benson, D.A., Meerschaert, M.M., Wheatcraft, S.W. (2001). Eulerian derivation of the fractional advection–dispersion equation. *Journal of Contaminant Hydrology*, *48*(1–2), 69–88, https://doi.org/10.1016/S0169-7722(00)00170-4

Sharan, M., Yadav, A.K., Modani, M. (2002). Simulation of short-range diffusion experiment in low-wind convective conditions. *Atmospheric Environment*, *36*, 1901–1906,

Silva, J.R.D., Xavier, P.H.F., Moreira, D.M. (2025). Near-field atmospheric dispersion modeling: a new approach for the two-dimensional steady-state advection-diffusion equation using fractal derivative. *Pure and Applied Geophysics*, *182*(1),

223–233, https://doi.org/10.1007/s00024-024-03624-8

Sorbjan, Z. (1986). On similarity in the atmospheric boundary layer. *Boundary-Layer Meteorology*, *34*, 377–397,

Stull, R.B. (1984). Transilient turbulence theory. Part I: the concept of eddy-mixing across finite distances. *Journal of the Atmospheric Sciences*, *41*(23), 3351–3367, https://doi.org/10.1175/1520-0469(1984)041⟨3351:TTTPIT⟩2.0.CO;2

Tankou Tagne, A.S., Ele Abiama, P., Ema'a Ema'a, J.M., Owono Ateba, P., Ben-Bolie, G.H. (2021). A three-dimensional fractional solution for air contaminants dispersal in the planetary boundary layer. *Heliyon*, *7*(5), e07005, https://doi.org/10.1016/j.heliyon.2021.e07005

Troparevsky, M.I., Muszkats, J.P., Seminara, S.A., Zitto, M.E., Piotrkowski, R. (2022). Modeling particulate pollutants dispersed in the atmosphere using fractional turbulent diffusion. *Physica A*, *599*, 127478, https://doi.org/10.1016/j.physa.2022.127478

Weil, J.C., Sullivan, P.P., Patton, E.G., Moeng, C.-H. (2012). Statistical variability of dispersion in the convective boundary layer: ensembles of simulations and observations. *Boundary-Layer Meteorology*, *145*(1), 185–210, https://doi.org/10.1007/s10546-012-9704-y

968 Willis, G.E., & Deardorff, J.W. (1976). A laboratory model of diffusion into the con-
969 vective planetary boundary layer. *Quarterly Journal of the Royal Meteorological*
970 *Society*, *102*, 427–445,
971

972 Zilitinkevich, S.S. (1972). On the determination of the height of the Ekman boundary
973 layer. *Boundary-Layer Meteorology*, *3*, 141–145,
974

Supplementary Files

This is a list of supplementary files associated with this preprint. Click to download.

- Table1.tex
- Table2.tex
- Table3.tex
- Table4.tex
- Table6.tex
- Table8.tex
- Table9.tex
- TableA1.tex
- TableA3.tex
- TableA5.tex
- OnlineResource1.tex